Analysis of Flicker Caused by Large Electronic Loads in Weak Power Grids

Eliot Jiménez-Ortega and Surya Santoso
The University of Texas at Austin
Austin, USA

Robert F. Arritt
Electric Power Research Institute
Palo Alto, USA

***Abstract*—Large electronic loads (LELs), such as artificial-intelligence (AI) data centers, are one of the most rapidly growing class of electric loads. They are characterized by highly variable and fast-ramping power consumption, which can significantly degrade power quality in electrical systems. This paper investigates LEL-induced voltage flicker caused by power fluctuations in hyperscale AI data centers (HAIDCs) under varying short-circuit capacity (SCC) conditions. The fundamental concept of SCC is first revisited to highlight its role in limiting voltage fluctuations. The operation of the flickermeter is then examined to illustrate how flicker severity is influenced by both the amplitude and the frequency content of the HAIDC power fluctuations. A current-source-based load model is developed from a real HAIDC demand profile and evaluated in EMTP across multiple power system scenarios. Results show that both the system strength and the frequency of the power fluctuations associated with the training activity determine the flicker severity, with the highest values consistently observed within the 6–12 Hz range. Furthermore, ramp-up events at the onset of training runs introduce additional transient flicker components that can contribute to overall flicker severity by more than 50%, particularly as fluctuation frequencies move away from the 6–12 Hz range.**

***Index Terms*—data center, flicker, power quality, voltage fluctuations**

I. Introduction

As renewable generation displaces synchronous machines, power systems will become increasingly dominated by inverter-based resources (IBRs). Unlike synchronous generators (SGs), IBRs lack inherent mechanical inertia and provide limited short-circuit current, which reduces both system strength and inertial response in power grids. This transition introduces new operational and stability challenges for emerging grids [1].

In this context, the interconnection of large electronic loads (LELs) such as hyperscale artificial-intelligence data centers (HAIDCs), one of the fastest-growing categories of large loads, can further exacerbate these challenges [2]. These facilities are composed of multiple high-performance compute nodes that integrate multiple graphics processing units (GPUs) as their computational cores [3]. In contrast to conventional data centers, the electrical demand behavior of AI-driven facilities presents different operational modes corresponding to different stages in their development and use, such as the training and inference phases [2], [4]. During large-scale model training, power demand can fluctuate sharply due to the synchronous operation of GPU clusters and periodic checkpoint operations that save model parameters. These rapid variations can occur within sub-second timescales, producing steep ramp rates and transient power surges [3].

As the interconnection of these emerging loads coincides with the transition from conventional synchronous generation to IBR-dominated grids, understanding their impact on power quality has become increasingly important. Several adverse effects can arise from the power swings generated by HAIDCs, such as grid instability and harmonic distortion [5]. Moreover, the rapidly fluctuating load profiles of AI-driven facilities can contribute to LEL-induced voltage flicker (hereafter referred to as flicker) [6]. While flicker produced by conventional fluctuating loads such as electric-arc furnaces has been extensively investigated, theoretical studies on the impact of flicker stemming from HAIDCs remain at an initial stage.

This paper investigates flicker induced by hyperscale AI data centers under varying short-circuit capacity (SCC), and power-fluctuation characteristics. First, the concept of SCC in the context of voltage fluctuation mitigation is revisited. Next, the flickermeter mechanism is reviewed to show how the characteristics of the HAIDC voltage fluctuations determine flicker severity. A current-source-based HAIDC load representation is developed from a real demand profile, and its flicker response is evaluated across multiple scenarios using a representative EMTP simulation model. Results show that flicker severity is dictated by both the SCC at the point of interconnection and the dominant fluctuation frequencies. Rapid ramp-up transitions add an additional transient component, which can increase overall flicker severity by more than 50%.

We begin our analysis in Section II by developing a realistic HAIDC demand profile. In Section III, the fundamental concept of SCC is revisited to highlight its role in limiting voltage fluctuations. Similarly, the role of frequency and magnitude of power demand fluctuations in flicker generation is analyzed. Section IV presents the simulation results and discussion. Finally, Section V concludes the paper.

II. Hyperscale AI Data Center Power Demand Modeling

HAIDCs commonly have capacities between 50 MW and 300 MW, while large campuses are expected to surpass 600 MW. A real power demand profile reported in [2] represents a 50 MW segment of a 200 MW AI training data center at the onset of a training cycle. The profile presents

979-8-3315-8138-1

characteristic ramping and fluctuation patterns of large-scale GPU workloads. At the start of training, power demand rises sharply from idle to near nominal, reaching about 1.9 p.u./s within 250 ms. During active training, the load remains high but shows rapid fluctuations and jitter spikes caused by alternating compute- and communication-intensive phases.

Based on this demand profile, a synthetic power profile was developed to emulate the behavior of hyperscale data centers, as shown in Fig. 1. The profile was scaled to a 400 MW base while preserving the per-unit ramp rate and fluctuation magnitude reported in [2]. The 2-minute, 1 ms-resolution waveform alternates between low ($\approx$ 48 MW or 0.12 pu) and high ($\approx$ 228 MW or 0.57) plateaus connected by rapid linear ramp of 1.9 pu/s during 250 ms. Since detailed information on the power fluctuation frequencies is not available, a band-limited stochastic jitter was superimposed on the waveform to emulate the demand variability reported as occurring on millisecond timescales [3]. The jitter was limited to narrow frequency bands, varied between 0.5 and 36 Hz, as described in Section IV. Finally, random short dips and spikes during high-power periods and small upward spikes during low-power intervals were introduced following Poisson statistics to replicate the observed demand behavior in [2].

Assuming a constant line-to-line voltage of 34.5 kV, the three-phase RMS currents are computed from the synthetic demand profile in Fig. 1 as

$$I_{\text{rms}}(t) = \frac{P(t)}{\sqrt{3}\, V_{\text{LL,rms}} \cos\theta}, \tag{1}$$

where the voltage is assumed constant to ensure that any fluctuations originate only from the load behavior, and the power factor is set to 0.98. These current waveforms are then imported into EMTP to reproduce the dynamic behavior of the HAIDC. For the simulations presented, the first two minutes of data were used to capture representative power fluctuations.

Fig. 2 illustrates the voltage response to the synthetic demand profile. The normalized, instantaneous phase voltage and the RMS voltage show that, when the HAIDC load ramps up at the start of the training phase, the increased active power

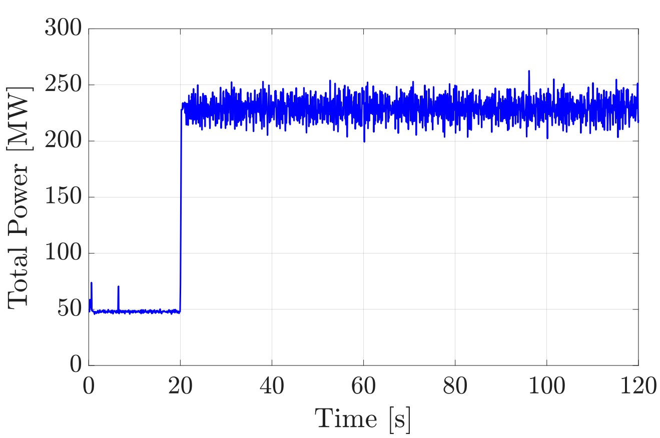

Fig. 1. Synthetic demand profile of a hyperscale AI data center derived from the profile reported in [2], showing rapid ramping and high-frequency power fluctuations characteristic of GPU-based training.

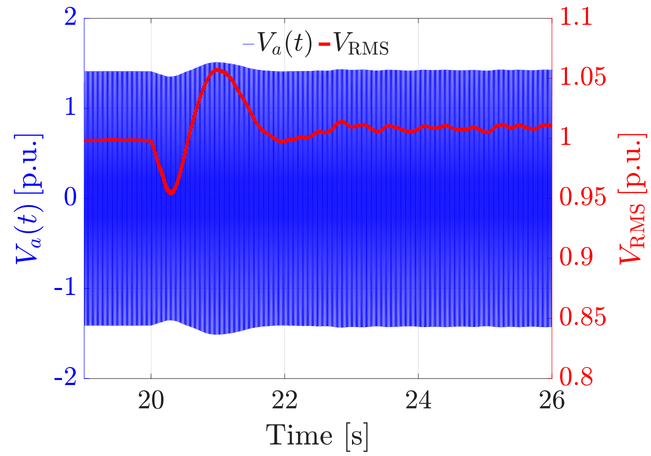

Fig. 2. Normalized phase and RMS voltages during the ramp-up event of the HAIDC demand.

demand causes a temporary voltage sag due to the voltage drop across the system's impedance. The SGs then react through excitation and governor control, providing reactive and active power support. This response leads to a brief voltage overshoot before the system settles to a new steady operating point, after which the steady fluctuations corresponding to the active training phase become visible. This voltage behavior corresponds to the one observed in the simulation model introduced in Section IV.

III. Grid Strength and Load Fluctuation Effects on Flicker Severity

This section revisits the fundamental concept of short-circuit capacity in the context of both synchronous generators and IBRs and examines its influence on voltage fluctuations. Furthermore, the impact of voltage fluctuation magnitude and frequency on the perceived flicker level is analyzed.

A. Short-Circuit Capacity

The SCC indicates the system's ability to supply current during faults. Synchronous generators typically contribute fault currents of up to 4 p.u., whereas IBRs are commonly limited to around 1.2 p.u. [7]. In such systems, the effective grid strength is also influenced by inverter control dynamics. Systems with higher SCC present smaller voltage deviations for a given load change and are therefore considered electrically stronger. The following formulation illustrates this relationship.

The SCC at a given bus can be expressed in terms of the rated line-to-line voltage and the Thevenin equivalent reactance as

$$SCC = \frac{V_{\text{LL}}^2}{X_{\text{th}}}, \tag{2}$$

To examine how SCC and ΔP affect voltage, consider a fluctuating load with primarily active power demand. Under linearized conditions, the current change can be expressed as

$$\Delta I \approx \frac{\Delta P}{\sqrt{3} V_{LL}}. \tag{3}$$

979-8-3315-8138-1

Using (2), the resulting voltage deviation through the Thevenin reactance X_{Th} is

$$\Delta V \approx \frac{\Delta P}{\sqrt{3}V_{LL}} \cdot \frac{V_{LL}^2}{SCC} = \frac{\Delta P}{\sqrt{3}} \cdot \frac{V_{LL}}{SCC}. \quad (4)$$

This relationship indicates that voltage fluctuations and, thus, flicker severity can be directly affected by the SCC at the POC of the fluctuating load. Consequently, in systems dominated by IBRs, the integration of large fluctuating loads such as HAIDCs represent an increased risk of voltage flicker.

B. Fluctuation Magnitude and Frequency

Voltage flicker refers to voltage variations that produce perceptible fluctuations in lamp brightness. Its severity depends on human visual sensitivity and is strongly influenced by the fluctuation frequency. Perceptible flicker occurs within the 0.5–30 Hz range, with peak sensitivity between 5 and 10 Hz, while lower frequencies present reduced perceptibility and higher frequencies are increasingly attenuated by the flickermeter weighting [8].

Flicker severity is typically quantified using standardized flickermeters that analyze the instantaneous voltage waveform and compute a flicker severity index through a defined demodulation, filtering, and statistical evaluation process [8]. The widely used IEC flickermeter performs this process through five functional blocks [9], [10]. The following analysis examines how the fluctuation frequency and magnitude affects flicker severity across these blocks.

The phase voltage from Fig. 2 can be generically modeled as a fundamental component at frequency $f_0 = 60$ Hz whose amplitude is slowly modulated by two envelope terms: a finite-duration transient associated with the load ramp at the start of the training phase, and a continuous low-frequency fluctuation during active training operation. Accordingly, the instantaneous voltage can be expressed as

$$v_{\mathrm{a}}(t) = \sqrt{2}\,V_0\big[\,1 + d_{\mathrm{ramp}}(t) + d_{\mathrm{train}}(t)\,\big]\cos\!\big(\omega_0 t + \phi\big), \quad (5)$$

where V_0 is the nominal RMS phase voltage, $\omega_0 = 2\pi f_0$, and ϕ is the fundamental phase angle.

The transient component associated with the rapid power ramp of the training activation can be modeled as a finite-duration modulation with a larger magnitude and a different dominant fluctuation frequency:

$$d_{\mathrm{ramp}}(t) = \begin{cases} M_{\mathrm{r}}\cos\!\big(\omega_{\mathrm{r}} t + \phi_r\big), & t_1 \le t \le t_2, \\ 0, & \text{otherwise.} \end{cases} \quad (6)$$

M_{r} denotes the modulation depth during the transient ramp event, $\omega_{\mathrm{r}} = 2\pi f_{\mathrm{r}}$ characterizes the dominant fluctuation frequency of the ramp, and $[t_1, t_2]$ defines the time interval over which the transient occurs.

The steady fluctuation component is represented as a superposition of low-frequency components associated with the sub-second oscillations and jitter spikes of the active training:

$$d_{\mathrm{train}}(t) = \sum_{k=1}^{K} m_{\mathrm{k}} \cos\!\big(\omega_{\mathrm{k}} t + \alpha_{\mathrm{k}}\big), \quad (7)$$

where m_{k} are modulation depths and α_{k} are their phase angles. The formulation in (5)–(7) adopts an amplitude-modulated representation, where voltage fluctuations relevant to flicker occur on time scales slower than the fundamental frequency and are modeled as envelope variations of the nominal sinusoidal voltage. The envelope terms separately capture the transient ramp event and the steady training-phase fluctuations observed in the actual HAIDC demand profile.

As the phase voltage $v_{\mathrm{a}}(t)$ is processed by the flickermeter, Block 1 first normalizes the input to an internal reference. Block 2 then demodulates the signal by squaring it, extracting the low-frequency amplitude modulation associated with perceptible brightness variation [8]. Block 3 filters this demodulated signal to retain only the envelope components relevant to flicker perception and applies a weighting filter that models the frequency-dependent sensitivity of the human visual system. This weighting strongly emphasizes modulation frequencies in the 5–10 Hz range, where flicker is most noticeable, and attenuates frequencies outside the perceptible band. Therefore, from (7) and (6), modulation components whose fluctuation frequencies ω_{k} or ω_{r} lie within this sensitivity range contribute more significantly to the resulting instantaneous flicker level, and their influence increases with modulation depths m_{k} and M_{r}. Finally, Blocks 4 and 5 model the nonlinear eye–brain response and statistically evaluate instantaneous flicker to determine the final severity index.

IV. Simulation Results and Flicker Severity Analysis

Consider the EMTP simulation model shown in Fig. 3. The system represents a 230 kV transmission network in which the power grid is modeled using a Thevenin equivalent, connected in parallel with four 250 MVA, 13.8 kV synchronous generators to represent the aggregate inertia and short-circuit capacity. A three-phase current source device that follows the demand of the profile defined in Section II represents an HAIDC facility, which is connected to the transmission grid through transmission line TLM1. The following three system configurations are evaluated:

- **Base Case:** The HAIDC load is connected to Bus L through TLM1.
- **SG Case:** Building on the Base configuration, a 13.8 kV, 75 MW synchronous generator with inertia constant $H = 8$ s is added at Bus L via TLM2, increasing system strength while keeping all other parameters unchanged.
- **PV Case:** The synchronous generator in the SG case is replaced by a 34.5 kV, 75 MW PV plant connected to Bus L through TLM2 and interfaced via a grid-following inverter with voltage/reactive power control, which can partially mitigate voltage fluctuations.

For each case, six simulations varied the power fluctuation frequency during the HAIDC active training phase across six

979-8-3315-8138-1

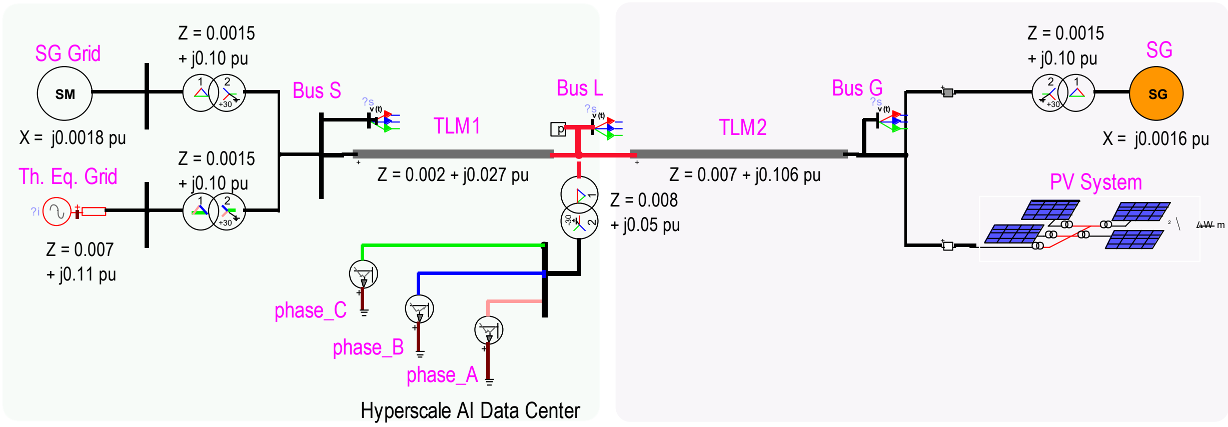

Fig. 3. EMTP simulation model of a an hyperscale AI data center facility connected to a 230 kV power system via a transmission line (TLM1). The power system is represented by a Thevenin equivalent in parallel with four 250 MVA, 13.8 kV, synchronous generators.

ranges while keeping the ramp event identical. The frequency ranges are 0.5–6, 6–12, 12–18, 18–24, 24–30, and 30–36 Hz. The duration of the simulations was set to 2 minutes and the resulting short-term flicker severity, P_{st}, was measured at Bus S and Bus L. Although P_{st} is defined over a 10-minute interval [10], applying the same 2-minute power variation across all cases provides a consistent basis for comparing relative flicker severity. Moreover, because P_{st} depends on relative voltage variations, the flicker results are governed by the short-circuit strength at the POI rather than by the nominal voltage level.

Simulation results are summarized in Table I. For reference, the Base Case P_{st} values at Bus S and Bus L for a non-fluctuating load of the same size are 0.8042 and 0.8296, respectively. Across all cases, the highest P_{st} values are observed for Range 2 (6–12 Hz), corresponding to the frequency band to which the human eye is most sensitive. As the dominant fluctuation frequency increases beyond this range, P_{st} gradually decreases, indicating reduced flicker severity for faster fluctuations. Similarly, in all cases, P_{st} is higher at Bus L than at Bus S, due to the shorter electrical distance to the load and the correspondingly lower short-circuit capacity at Bus L. Furthermore, among the different system configurations, the Base and PV cases consistently exhibit the highest P_{st} values due to their reduced SCC. In contrast, the SG case yield the lowest P_{st}, which confirms the mitigating effect of a stronger grid on voltage variations. The corresponding graphical comparison for all simulation cases is presented in Fig. 4.

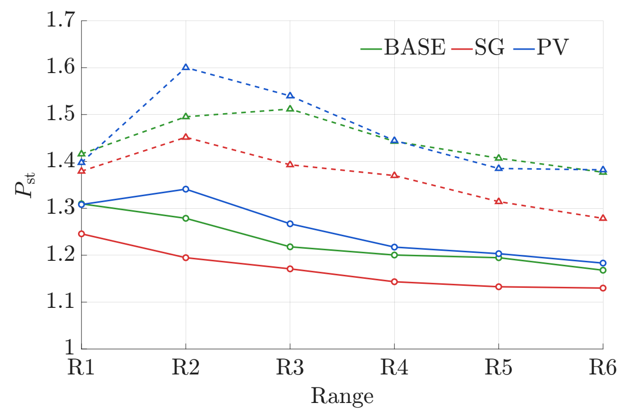

Fig. 4. Short-term flicker severity P_{st} across fluctuation-frequency ranges (0.5–36 Hz). Solid and dashed lines correspond to Bus S and Bus L, respectively. Stronger grids show lower P_{st} due to higher SCC.

A. *Contribution of Ramp Events to Flicker Severity*

As discussed in Section II, two of the main contributors to the measured P_{st} values in Table I are: (i) the ramp-up transient occurring at $t = 20$ s corresponding to the start of the training phase, and (ii) the subsequent steady fluctuations in power demand associated with the alternating compute and data-exchange phases of the training stage. This subsection quantifies the individual contribution of the ramp event.

The ramp-up event introduces a large, abrupt voltage change over a short duration of 250 ms, resulting in a pronounced but brief flicker component. Conversely, the steady fluctuations produce smaller, continuous variations in voltage magnitude

TABLE I
P_{st} RESULTS AT BUS S

	Case	H_{sys} [s]	SCC [MVA]	R1 0.5-6 Hz	R2 6-12 Hz	R3 12-18 Hz	R4 18-24 Hz	R5 24-30 Hz	R6 30-36 Hz
Bus S	Base	20	5,354	1.3096	1.2787	1.2179	1.2004	1.1947	1.1680
	SG	28	5,628	1.2456	1.1947	1.1709	1.1434	1.1327	1.1299
	PV	20	5,441	1.3081	1.3409	1.2670	1.2173	1.2033	1.1832
Bus L	Base	20	2,239	1.4160	1.4953	1.5118	1.4429	1.4069	1.3769
	SG	28	2,534	1.3792	1.4515	1.3929	1.3699	1.3143	1.2786
	PV	20	2,288	1.3977	1.6002	1.5398	1.4446	1.3850	1.3821

979-8-3315-8138-1

distributed across the defined frequency ranges, which contributes to the sustained portion of the flicker severity.

Let $P_{\mathrm{st}}^{\mathrm{total}}$ be the flicker severity measured during both the ramp and steady fluctuation stages of the HAIDC demand, which can be expressed as a cubic summation of two independent flicker sources as [11]

$$\left(P_{\mathrm{st}}^{\mathrm{total}}\right)^3 = \left(P_{\mathrm{st}}^{\mathrm{ramp}}\right)^3 + \left(P_{\mathrm{st}}^{\mathrm{fluct}}\right)^3, \tag{8}$$

where $P_{\mathrm{st}}^{\mathrm{fluct}}$ is the flicker from steady fluctuations alone, and $P_{\mathrm{st}}^{\mathrm{ramp}}$ the flicker attributable to the ramp event only. Given $P_{\mathrm{st}}^{\mathrm{total}}$ and $P_{\mathrm{st}}^{\mathrm{fluct}}$, $P_{\mathrm{st}}^{\mathrm{ramp}}$ can be then obtained as

$$P_{\mathrm{st}}^{\mathrm{ramp}} = \left[\left(P_{\mathrm{st}}^{\mathrm{total}}\right)^3 - \left(P_{\mathrm{st}}^{\mathrm{fluct}}\right)^3\right]^{1/3}. \tag{9}$$

Finally, following the cubic normalization of $P_{\mathrm{st}}^{\mathrm{total}}$ implied by (8), the relative contribution of the ramp event to the total flicker severity can be estimated as

$$\alpha = \frac{\left(P_{\mathrm{st}}^{\mathrm{ramp}}\right)^3}{\left(P_{\mathrm{st}}^{\mathrm{total}}\right)^3} = 1 - \left(\frac{P_{\mathrm{st}}^{\mathrm{fluct}}}{P_{\mathrm{st}}^{\mathrm{total}}}\right)^3. \tag{10}$$

The heatmap in Fig. 5 illustrates the percentage contribution of the ramp-up event to the total flicker severity at Bus L. The results indicate that the ramp event is a dominant contributor to flicker severity across all frequency ranges and system configurations. The lowest contributions are observed in R2, where the steady voltage fluctuations lie within the most perceptible frequency band and thus have a greater influence on overall flicker severity. The contribution of the ramp event increases outside this band, where the reduced perceptibility of steady fluctuations results in high ramp contributions that exceed 60% in R1 and R4–R5, and 70% in R6. This behavior is consistent with the established frequency-dependent response of the flickermeter, in which sensitivity peaks near 5–10 Hz and decreases toward lower and higher frequencies [8], as shown in Fig. 4.

Furthermore, averaged across all six frequency ranges, the percent contribution to flicker severity due to the ramp event is 64.3% for the Base case, 61.1% for the SG case, and 60.1% for the PV case. This indicates that the contribution of the ramp event is higher in electrically weaker systems. However, the similar averages observed in the SG and PV cases suggest that inverter-based resources can partially mitigate the impact of ramp events through their voltage control capabilities.

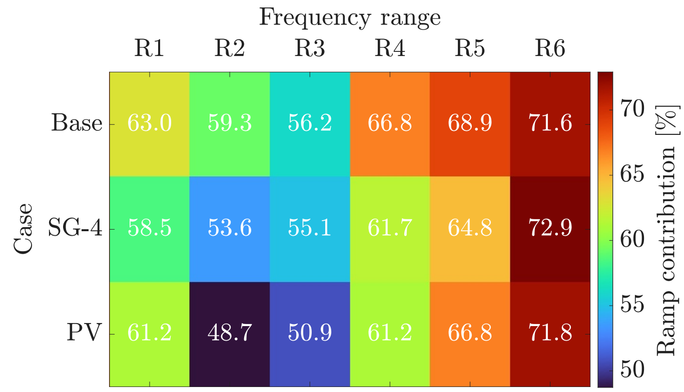

Fig. 5. Percentage contribution of the ramp event in short-term flicker severity at Bus L across all fluctuation frequency ranges and system configurations.

V. Conclusion

This paper presented an assessment of LEL-induced voltage flicker from hyperscale AI data centers using a current-source model derived from a real demand profile and evaluated under varying fluctuation frequencies and system configurations. It was shown that flicker severity strongly depends on the SCC of the system as well as the dominant frequencies of the power fluctuations associated with the active training phase. The highest P_{st} occurs in the 6–12 Hz range, which corresponds to the frequency band of peak human visual sensitivity to light fluctuations. Similarly, ramp-up events associated with the onset of the training phase are a major driver of flicker and can become the dominant contributor to short-term flicker severity. Although the numerical results are specific to the scenarios examined in this paper, the identified flicker mechanisms are broadly applicable. Future work will focus on quantifying sensitivity to parameters including ramp rate, load level, transmission line length, power factor, reactive compensation, and penetration of IBRs.

References

[1] WECC Renewable Energy Modeling Task Force, Western Electricity Coordinating Council Modeling and Validation Work Group, *WECC PV Power Plant Dynamic Modeling Guide*, Apr. 2014. [Online]. Available: https://www.wecc.biz/Reliability/WECC Solar Plant Dynamic Modeling Guidelines.pdf.

[2] North American Electric Reliability Corporation (NERC), "Characteristics and risks of emerging large loads," North American Electric Reliability Corporation, White Paper, July 2025, prepared by the NERC Large Loads Task Force.

[3] Y. Li, M. Mughees, Y. Chen, and Y. R. Li, "The unseen AI disruptions for power grids: Llm-induced transients," 2024, submitted 9 Sep 2024. [Online]. Available: https://arxiv.org/abs/2409.11416

[4] L. H. Kaack, P. L. Donti, E. Strubell, G. Kamiya, F. Creutzig, and D. Rolnick, "Aligning artificial intelligence with climate change mitigation," *Nature Climate Change*, vol. 12, no. 6, pp. 518–527, Jun. 2022. [Online]. Available: https://doi.org/10.1038/s41558-022-01377-7

[5] R. R. Ahrabi, A. Mousavi, E. Mohammadi, R. Wu, and A. K. Chen, "AI-driven data center energy profile, power quality, sustainable sitting, and energy management: A comprehensive survey," in *2025 IEEE Conference on Technologies for Sustainability (SusTech)*, 2025, pp. 1–8.

[6] A. Azizi, A. Aluko, S. Maleki, R. Salehi, and H. Bayat, "Grid-forming inverter applications for improved reliability and power quality in ai data centers," in *2025 IEEE Power & Energy Society General Meeting (PESGM)*, 2025, pp. 1–5.

[7] C. Henderson, A. Egea-Alvarez, T. Kneuppel, G. Yang, and L. Xu, "Grid strength impedance metric: An alternative to scr for evaluating system strength in converter dominated systems," *IEEE Transactions on Power Delivery*, vol. 39, no. 1, pp. 386–396, 2024.

[8] R. C. Dugan, M. F. McGranaghan, S. Santoso, and H. W. Beaty, *Electrical Power Systems Quality, Third Edition*, 3rd ed. McGraw-Hill Education, 2012. [Online]. Available: https://www.accessengineeringlibrary.com/content/book/9780071761550

[9] *Electromagnetic compatibility (EMC) – Part 4-15: Testing and measurement techniques – Flickermeter – Functional and design specifications*, International Electrotechnical Commission Std. IEC 61 000-4-15, 2010, edition 2.0.

[10] "IEEE standard for measurement and limits of voltage fluctuations and associated light flicker on ac power systems," *IEEE Std 1453-2022 (Revision of IEEE Std 1453-2015)*, pp. 1–83, 2022.

[11] H. Renner and M. Sakulin, "Flicker propagation in meshed high voltage networks," in *Ninth International Conference on Harmonics and Quality of Power. Proceedings (Cat. No.00EX441)*, vol. 3, 2000, pp. 1023–1028.

979-8-3315-8138-1